

*Distribution A: Approved for public release: distribution unlimited.*

# **Wave Exposure on the Northern Coast of Alaska Using the SWAN Model with a Sea Ice Parameterization**

by Lucia Hošeková (Univ. Hawaii), W. Erick Rogers (Naval Research Laboratory, Code 7322),  
and Jim Thomson (APL-UW)

Technical Report  
**APL-UW TR 2302**  
May 2023



**Applied Physics Laboratory University of Washington**  
1013 NE 40th Street Seattle, Washington 98105-6698

*Grants: National Science Foundation OPP-1818485  
and Office of Naval Research N00014-20-W-X-01935*

## ACKNOWLEDGMENTS

This work was funded by the National Science Foundation (OPP-1818485) and the Office of Naval Research (N00014-20-W-X-01935) as part of the Coastal Ocean Dynamics in the Arctic program ([www.apl.washington.edu/coda](http://www.apl.washington.edu/coda)). The original field data collection was funded by the Office of Naval Research (N00014-12-1-0113) as part of the Marginal Ice Zone program ([www.apl.uw.edu/miz](http://www.apl.uw.edu/miz)). This is Naval Research Laboratory contribution number NRL/OT/7320-23-5894. This work was initiated by our late colleague, Prof. Nirnimesh Kumar, who is dearly missed.

## **ABSTRACT**

The presence of sea ice along Arctic coastlines controls the exposure of the coast to wave action. We present a case study from the summer of 2014 to demonstrate the recent addition of ice attenuation in the SWAN (Simulating WAVes Nearshore) numerical wave model. Observations from several freely drifting SWIFT (Surface Wave Instrument Float with Tracking) buoys show reduced wave action resulting from remnant sea ice along the coast in early summer. This is well-described by the new model that includes sea ice attenuation, relative to a previous version of the wave model without a sea ice parameterization. The model is sensitive to the sea ice product used for model initialization because some sea ice products do not resolve coastal ice. The difference in the cumulative wave exposure at the coast shows that sea ice attenuation in early summer is a significant seasonal effect.

# 1 INTRODUCTION

Arctic coasts are eroding with an average shoreline position retreat of 0.5 m/yr (*Lantuit et al.*, 2012). The northern coast of Alaska bordering the Chukchi and the Beaufort seas has an even higher regional average shoreline retreat rate of 1.4 m/yr (*Gibbs et al.*, 2015). The high erosion rates are driven, in part, by melting permafrost in the presence of warming waters (*Jones et al.*, 2009). The mechanical action of waves is also an important driver of coastal change (*Overeem et al.*, 2011). There is a clear trend of increasing surface wave activity in the Arctic (*Thomson et al.*, 2016, 2018b; *Wang et al.*, 2016), which motivates the development and application of wave–ice coupled coastal models. The increasing wave trend is related directly to the expanding fetch distances available for surface wave development during the expanding open-water season (*Smith and Thomson*, 2016; *Thomson and Rogers*, 2014). The presence of any sea ice near the coast attenuates the incoming waves (*Squire*, 2007; *Squire et al.*, 1995; *Thomson*, 2022) providing the coast partial protection. When sea ice persists along the coast in the early summer, this attenuation can reduce the cumulative seasonal wave exposure at the coast (*Hosekova et al.*, 2021).

Here, we apply a recent version of the SWAN (Simulating WAVes Nearshore) numerical wave model that includes a sea ice parameterization (*Rogers*, 2019) to a case study of the Alaska Arctic coast in 2014. The summer of 2014 was selected because remnant sea ice persisted along the coast well into August. Ice products from the U.S. National Ice Center show coastal sea ice in early August, when the coast is typically ice-free (Figure 1). By late August 2014 this coastal ice disappeared. Ground truth observations for the 2014 case study are provided by several drifting wave buoys. The new SWAN model reproduces the effects of this remnant ice. Section 2 describes the observations and section 3 the model and inputs (especially ice products), section 4 presents our results (including cumulative wave exposure), and concluding remarks are presented in section 5.

## 2 WAVE OBSERVATIONS

Two SWIFT buoys were deployed off the northern coast of Alaska in August 2014 as part of the Office of Naval Research Marginal Ice Zone program ([www.apl.uw.edu/miz](http://www.apl.uw.edu/miz)). The SWIFTs (hull numbers 10 and 11) were deployed in the open water at the shelf break, approximately 50 km from the coast, and were allowed to drift freely for two months (*Smith and Thomson, 2016*). A third SWIFT (hull number 12) was deployed in Stefansson Sound, near Prudhoe Bay, on August 2 downwind of a sea ice patch that had persisted along the coast. Satellite telemetry provided tracking and realtime data from all SWIFT buoys (Figure 2).

The SWIFT 12 deployment in Stefansson Sound was an opportunistic study of fetch evolution. Over the course of 6 hr, SWIFT 12 was repeatedly re-positioned and redeployed at increasing distances from the remnant ice to observe fetch dependence of wind waves in the presence of partial ice cover. Fourteen buoy deployments were recorded, each 10 min in duration and in increments of every 1.8 km from the ice edge (Figure 3).

SWIFT buoys measure waves using a combination of GPS velocities and inertial measurement units (*Herbers et al., 2012; Thomson, 2012; Thomson et al., 2018a*). The standard bulk parameters of significant wave height, peak wave period, and dominant wave direction are estimated from the standard scalar energy spectra and directional moments of the spectra. The noise level in the energy spectra is approximately  $10^{-4}$  m<sup>2</sup>/Hz, which results in a significant wave height uncertainty of  $\pm 0.05$  m.

SWIFTs also measure winds (1 m height), water temperature (0.5 m depth), and salinity (0.5 m depth). Salinity increased with distance along fetch and away from the ice during the SWIFT 12 experiment (not shown).

### 3 SWAN MODEL

Evaluation of the SWAN [Simulating WAVes Nearshore, *Booij et al. (1999)*] model is the primary focus of this study. We also use WAVEWATCH III [WW3, *The WAVEWATCH III® Development Group (WW3DG) (2016); Tolman (1991)*] to provide boundary forcing for our SWAN implementation (section 3.2). Both are phase-averaged spectral models, for which the prognostic variable is wave action spectral density, which is the wave energy spectral density divided by the angular wave frequency:  $N = E/\sigma$ , where  $\sigma = 2\pi f = 2\pi/T$  ( $T$  denoting wave period). The spectrum is a function of wavenumber or angular frequency ( $k$  or  $\sigma$ ), direction ( $\theta$ ), space ( $x, y$  or longitude, latitude), and time ( $t$ ). The left-hand side of the radiative transfer equation includes terms for the time rate of change and propagation in the four dimensions (kinematics), while the right-hand side provides source functions (dynamics):

$$\frac{\partial N}{\partial t} + \nabla \cdot \vec{c}N = \frac{S}{\sigma} \quad (1)$$

where  $\vec{c}$  is a four-component vector describing the propagation velocities in  $x, y, k$ , and  $\theta$ . For example, in the absence of currents,  $c_x$  is the  $x$ -component of group velocity  $C_g$ . The sum of all source functions is denoted as  $S$ , and individual source functions are indicated with an appropriate subscript:  $S_{in}$ ,  $S_{wc}$ ,  $S_{nl4}$ , and  $S_{ice}$  being energy input from wind, dissipation by whitecapping, four-wave nonlinear interactions, and dissipation by sea ice, respectively.

#### 3.1 SWAN source term parameterizations

For the primary open water input and dissipation terms,  $S_{in}$  and  $S_{wc}$ , we use the parameterization implemented in SWAN by *Rogers et al. (2012)*, with updates known as ST6. Swell dissipation (weak losses of energy not associated with breaking) is represented as negative wind input, following *Ardhuin et al. (2010)*. For four-wave nonlinear interactions,  $S_{nl4}$ , important for any wave hindcast with active wave growth, we use the Discrete Interaction Approximation (DIA) of *Hasselmann et al. (1985)*. Bottom friction is not activated.

Sea ice was introduced to the SWAN model by *Rogers (2019)*. Here,  $S_{ice}$  is scaled by areal ice fraction  $a_{ice}$ , following *Doble and Bidlot (2013)*. Ice cover is also expected to affect other source terms, though the true behavior is not well understood. The default behavior of SWAN is to scale open water source terms by the open water fraction,  $1 - a_{ice}$ :

$$S = (1 - a_{ice})(S_{in} + S_{wc} + S_{nl4}) + a_{ice}S_{ice} \quad (2)$$

The exponential decay rate of amplitude in the space domain is given by  $k_i$ , and the exponential decay rate of energy in the time domain, prior to scaling by  $a_{ice}$ , is computed as  $D_{ice} = S_{ice}/E = -2C_g k_i$ . The group velocity  $C_g$  can, in principle, be affected by ice cover, particularly in frequencies above 0.3 Hz (*Cheng et al., 2017; Collins et al., 2018*), but here we simply assume that the group velocity is the open water group velocity. The attenuation by sea ice,  $k_i$ , is parameterized using the IC4M2 parameterization implemented in SWAN by *Rogers (2019)*, which is based on an equivalent method implemented in WW3 by *Collins and Rogers (2017)*:

$$k_i = \alpha/2 = c_0 f^0 + c_1 f^1 + \dots + c_6 f^6 \quad (3)$$

Here,  $k_i$  has units of  $1/m$ ,  $f$  has units of Hz, and  $C_0, C_1$ , etc. are dimensional, e.g.,  $C_2$  has units of  $s^2 m^{-1}$ . (Though the two models use functionally equivalent formulas, the coefficient values and notation differ; see *Rogers (2019)* for more information.) The method of input in SWAN is:

```
IC4M2 [aice] [c0] [c1] [c2] [c3] [c4] [c5] [c6]
```

In our case, we use non-uniform ice concentration, so [aice] is ignored. We use the instruction:

```
IC4M2 1.0 0.0 0.0 1.06e-3 0.0 2.3e-2 0.0 0.0
```

Thus,  $C_2 = 1.06 \times 10^{-3}$  and  $C_4 = 2.3 \times 10^{-2}$ , following the report of *Meylan et al. (2014)* for broken floes in the Antarctic.

### 3.2 SWAN input fields, grid and numerical settings

Wind forcing in the form of 10-m wind vectors is from archives of the U.S. Navy global atmospheric model, NAVGEM (*Hogan and coauthors, 2014*), at 3-hourly intervals and  $1/2^\circ$  geographic resolution. (This resolution improved to  $1/4^\circ$  in July 2015, which is after the period of this study).

Input fields for areal ice fraction  $a_{ice}$  come from the U.S. Navy Arctic Cap Nowcast Forecast System (*Posey et al., 2015*) (ACNFS) at a resolution near 4 km. The second  $a_{ice}$  product for the nested grid is from AMSR2 analyses using the ARTIST algorithm (*Beitsch et al., 2014; Spreen et al., 2008*). This ice concentration product is at relatively high geographic resolution (median spacing is 3.05 km) but relatively low temporal resolution (one field every 24 hr).

The SWAN model hindcast was from 0000 UTC 1 August 2014 to 0000 UTC 29 Septem-

ber 2014, computed with a 6-min time step.

The SWAN model grid receives boundary forcing from a WW3 hindcast. The latter was run from 0000 UTC 25 July to 1200 UTC 30 September 2014. This WW3 grid has horizontal resolution of approximately 10 km, and is shown in Figures 4 and 5. The WW3 hindcast uses the source term package of *Ardhuin et al. (2010)* known as ST4, for  $S_{in}$  and  $S_{wc}$ . The bounds of the SWAN nest are indicated in Figure 6. The computational grid is irregular with 500 to 300 grid points and resolution varying from 0.35 to 4.06 km, with median resolution near 1.3 km.

The spectral grid has directional resolution of  $6^\circ$  and uses 49 frequency bins, logarithmically spaced, from 0.01 to 1.0 Hz. We use the original first order BSBT propagation scheme as described by *Booij et al. (1999)*.

### 3.3 Other sea ice products

Several other sea ice products were considered for the SWAN model runs. One from AMSR2 analyses was obtained from the National Snow and Ice Data Center (NSIDC) online portal (*Meier et al., 2018*). It provides sea ice concentration at 12.5-km resolution every 24 hr. The  $a_{ice}$  reported in the Beaufort Sea by AMSR2 and Navy Arctic Cap on 2 August 2014 are in good agreement (Figure 7). Both show regions with pack ice of high sea ice concentration ( $a_{ice} > 0.8$ ). The remnant coastal ice with  $a_{ice} < 0.8$  (Figure 1) is apparent in the Arctic Cap product but is not represented in AMSR2.

Other sea ice products considered as forcing datasets for the SWAN model were the EUMETSAT Ocean and Sea Ice Satellite Application Facility (OSI SAF), the Multisensor Analyzed Sea Ice Extent (MASIE), and manually generated ice charts. At 25-km resolution, OSI SAF has bias similar to AMSR2, omitting the low concentration of nearshore ice. MASIE is a high-resolution (4 km) sea ice extent product, and reports both pack ice and nearshore ice presence successfully. MASIE's applicability as a forcing product for SWAN is limited because it reports sea ice extent only rather than concentration needed by SWAN's ice source term  $S_{ice}$ . Finally, a manually gridded product was generated using ice charts from Figure 1 covering the regions of Beaufort Sea relevant for the Stefansson Sound SWIFT deployments to correct for the underreporting of nearshore ice in AMSR2. While labor intensive, this approach allowed us to reproduce the sea ice conditions for the duration of the 2–3 August experiment when combined with the AMSR2 dataset.

## 4 RESULTS

### 4.1 Model and observations compared

The SWAN model configuration (section 3.2) produced two runs targeting the domain and duration of the wave buoy deployments (section 2) in 2014. One of the runs utilized the IC4M2 method forced with the Arctic Cap model; the second run included no sea ice input, treating the domain as open water while using the same WW3 wave forcing at the boundary.

Maps of significant wave height output from the two runs for 2 August 2014, when remnant coastal ice was present and SWIFT 12 was deployed in Stefansson Sound, show the importance of coastal ice in reducing the observed wave heights. In some grid cells the difference is as much as 1.5 m (Figure 8).

Comparisons of the significant wave heights observed by SWIFT 10 at the Beaufort Sea shelf break to the ice/no ice SWAN runs are in good agreement (Figure 9, top) regardless of the ice scheme. For these offshore data, both model runs yield nearly identical results, because the wave heights were largely unaffected by the presence of sea ice along the buoy trajectory. The slight difference between the two runs ( $< 10\%$ ) during the first 10 days demonstrates the reduction in wave heights caused by ice upwind from the buoy location.

Comparison of the two SWAN runs with wave height observations by SWIFT 12 during the fetch experiment in Stefansson Sound on 2 August 2014 show an increasing trend (Figure 9, bottom), in accordance with the experiment setup where each of the 14 deployments was 1.8 km further downwind from the ice edge. In the ‘no ice’ configuration the model overestimates the observed wave heights by up to 400%, while the model with ice estimates the range of observed wave heights successfully. The model with ice does not capture the details of the fetch evolution, presumably because it is a sub-grid-scale process. With the sea ice product resolution at 4 km, SWAN estimates are poorly suited to reproduce the wave evolution over the observed 25 km fetch. Despite this, the model with ice has greater skill reproducing the *range* of observed wave heights. A histogram of observational and model output further highlights the statical skill of the sea ice scheme (Figure 10).

### 4.2 Coastal wave exposure

The SWAN model runs (section 4.1) provide a tool to quantify the effects of nearshore ice on coastal wave exposure. While buoy data are sparse, the model output has wave height

estimates at every hour at every location along the coast. We estimated the mean significant wave heights in the southern-most grid cell of the SWAN domain (introduced in Figure 6) that are  $> 10$  m deep (Figure 11, top). Given the coastal topography of northern Alaska, this simple approach provides a good method of identifying the coastal grid cells while excluding shallow water effects (e.g., shoaling, refraction, depth-limited breaking). The time series shows that the presence of nearshore ice resulted in a bulk reduction of about 0.5 m in wave heights during the first 12 days of August 2014.

Following *Hosekova et al.* (2021), we use a simple wave exposure metric,

$$\mathcal{X} = \int H_s \Delta t, \quad (4)$$

and estimate that the remnant sea ice resulted in 20% reduction in commutative coastal wave exposure during August 2014 (Figure 11, bottom). This highlights the importance of considering the nearshore and landfast sea ice presence when estimating wave activity for coastal applications, in particular during transition seasons when partial ice coverage provides sufficient wave fetch and sea-ice interactions become relevant (*Hosekova et al.*, 2021).

## 5 CONCLUSIONS

The report presents a case study comparing wave buoy data with a version of the SWAN wave model that includes attenuation by sea ice. We conclude:

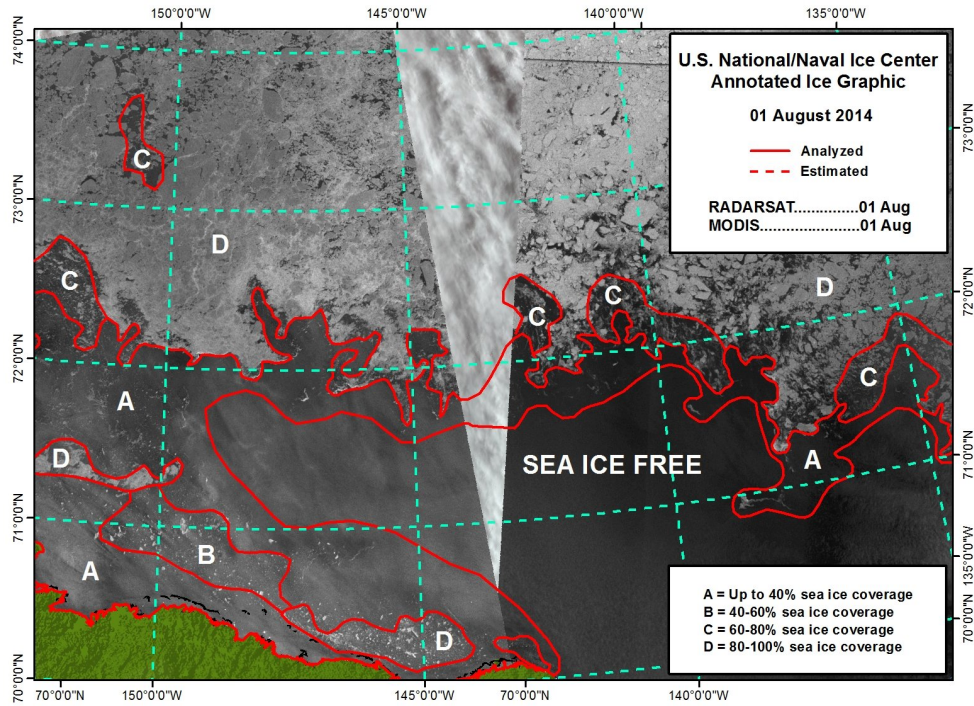
1. Incorporating the IC4M2 parametrization improves model skill in representing wave heights, relative to a baseline ‘no ice’ model (which overestimates wave heights by up to 400%).
2. The presence of remnant coastal ice in early summer affects the cumulative wave exposure at the coasts.
3. The resolution and accuracy of coastal sea ice products used as inputs to SWAN affect the accuracy of the results. The popular AMSR2 ice product is a particularly poor choice for coastal ice model input.
4. The biases between model results and observations can be attributed to limitations in the resolution of the ice product and presence of sea ice outside the model domain.

## REFERENCES

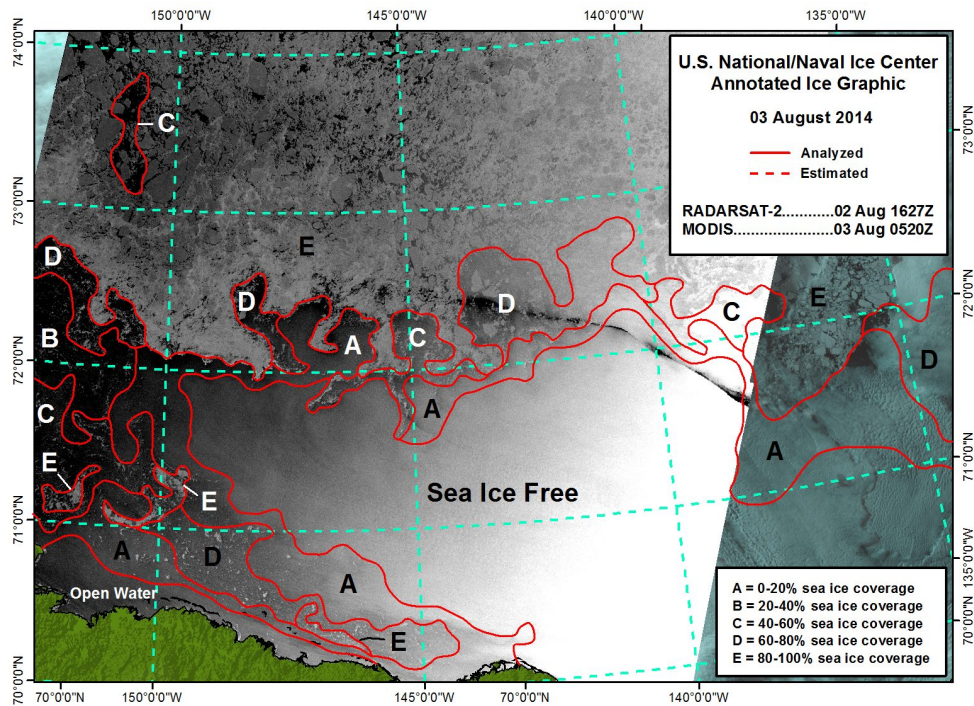
- Amante, C., and B.W. Eakins, ETOPO1 Arc-Minute Global Relief Model: Procedures, Data Sources and Analysis, *NOAA Technical Memorandum NESDIS NGDC-24*, National Geophysical Data Center, NOAA, doi:{10.7289/V5C8276M}, 326 pp. + Appendices, 2009.
- Ardhuin, F., et al., Semi-empirical dissipation source functions for ocean waves: Part I, definitions, calibration, and validations, *J. Phys. Oceanogr.*, *40*, 1917–1941, 2010.
- Beitsch, A., L. Kaleschke, and S. Kern, Investigating high-resolution AMSR2 sea ice concentrations during the February 2013 fracture event in the Beaufort Sea, *Remote Sens.*, *6*(5), 3841–3856, doi:{10.3390/rs6053841}, 2014.
- Booij, N., R. C. Ris, and L. H. Holthuijsen, A third-generation wave model for coastal regions, 1. Model description and validation, *J. Geophys. Res.*, *104*, 7,649–7,666, 1999.
- Cheng, S., et al., Calibrating a viscoelastic sea ice model for wave propagation in the Arctic fall marginal ice zone, *J. Geophys. Res.*, *122*, doi:10.1002/2017JC013275, 2017.
- Collins, C., and W. Rogers, A Source Term for Wave Attenuation by Sea ice in WAVEWATCH III®: IC4, *Tech. Rep. NRL/MR/7320–17-9726*, Naval Research Laboratory, 2017.
- Collins, C. O., H. Potter, B. Lund, H. Tamura, and H. C. Graber, Directional wave spectra observed during intense tropical cyclones, *J. Geophys. Res.*, *123*, doi:10.1002/2017JC012943, 2018.
- Doble, M. J., and J.-R. Bidlot, Wave buoy measurements at the Antarctic sea ice edge compared with an enhanced ECMWF WAM: Progress towards global waves-in-ice modelling, *Ocean Model.*, *70*(Supplement C), 166 – 173, doi:https://doi.org/10.1016/j.ocemod.2013.05.012, 2013.
- Gibbs, A., K. Ohman, and B. Richmond, National assessment of shoreline change—a GIS compilation of vector shorelines and associated shoreline change data for the north coast of Alaska, U.S.-Canadian border to Icy Cape, *Open-File Report 2015-1030*, U.S. Geological Survey, doi:10.3133/ofr20151030, 2015.
- Hasselmann, S., K. Hasselmann, J. H. Allender, and T. P. Barnett, Computations and parameterizations of the nonlinear energy transfer in a gravity-wave spectrum, Part II: Parameterizations of the nonlinear energy transfer for application in wave models, *J. Phys. Oceanogr.*, *15*, 1,378–1,391, 1985.
- Herbers, T. H. C., P. F. Jessen, T. T. Janssen, D. B. Colbert, and J. H. MacMahan, Observing ocean surface waves with GPS tracked buoys, *J. Atmos. Ocean. Technol.*, *29*, doi:10.1175/JTECH-D-11-00128.1, 2012.

- Hogan, T., and coauthors, The Navy Global Environmental Model, *Oceanography*, 27(3), 116–125, 2014.
- Hosekova, L., E. Eidam, G. Panteleev, L. Rainville, R. Erick, and J. Thomson, Landfast ice and coastal wave exposure in northern Alaska, *Earth Space Sci.*, doi:10.1002/essoar.10507727.1, 2021.
- Jones, B. M., C. D. Arp, M. T. Jorgenson, K. M. Hinkel, J. A. Schmutz, and P. L. Flint, Increase in the rate and uniformity of coastline erosion in Arctic Alaska, *Geophys. Res. Lett.*, 36(3), doi:10.1029/2008GL036205, 103503, 2009.
- Lantuit, H., et al., The Arctic Coastal Dynamics Database: A new classification scheme and statistics on Arctic permafrost coastlines, *Estuaries Coasts*, 35(2), 383–400, 2012.
- Meier, W. N., T. Markus, and J. C. Comiso, AMSR-E/AMSR2 Unified L3 daily 12.5 km brightness temperatures, sea ice concentration, motion & snow depth polar grids, Version 1, doi:10.5067/RA1MIJOYPK3P, 2018.
- Meylan, M. H., L. G. Bennetts, and A. L. Kohout, In situ measurements and analysis of ocean waves in the antarctic marginal ice zone, *Geophys. Res. Lett.*, 41, 5046–5051, doi:10.1002/2014GL060809, 2014.
- Overeem, I., R. S. Anderson, C. W. Wobus, G. D. Clow, F. E. Urban, and N. Matell, Sea ice loss enhances wave action at the Arctic coast, *Geophys. Res. Lett.*, 38(17), doi:10.1029/2011GL048681, 2011.
- Posey, P. G., et al., Improving Arctic sea ice edge forecasts by assimilating high horizontal resolution sea ice concentration data into the U.S. Navy’s ice forecast systems, *Cryosphere*, 9(), 1735–1745, doi:{10.5194/tc-9-1735-2015}, 2015.
- Rogers, W. E., Implementation of sea ice in the wave model SWAN, *Tech. Rep. 19-9874*, Naval Research Laboratory, 2019.
- Rogers, W. E., A. V. Babanin, and D. W. Wang, Observation-consistent input and whitecapping dissipation in a model for wind-generated surface waves: Description and simple calculations, *J. Atmos. Oceanic Technol.*, 29, 1329–1346, 2012.
- Smith, M., and J. Thomson, Scaling observations of surface waves in the Beaufort Sea, *Elem. Sci. Anth.*, 4, doi:10.12952/journal.elementa.000097, 2016.
- Spreen, G., L. Kaleschke, and G. Heygster, Sea ice remote sensing using AMSR-E 89-GHz channels, *J. Geophys. Res.*, 113(), doi:{10.1029/2005JC003384}, 2008.
- Squire, V. A., Of ocean waves and sea ice revisited, *Cold Regions Sci. Tech.*, 49, 110–133, 2007.

- Squire, V. A., J. P. Dugan, P. Wadhams, P. J. Rottier, and A. K. Liu, Of ocean waves and sea ice, *Annu. Rev. Fluid Mech.*, 27, 115–168, 1995.
- The WAVEWATCH III<sup>®</sup> Development Group (WW3DG), User manual and system documentation of WAVEWATCH III<sup>®</sup> version 5.16, *Tech. Note 329*, NOAA/NWS/NCEP/MMAB, College Park, MD, USA, 326 pp. + Appendices, 2016.
- Thomson, J., Wave Breaking Dissipation Observed with fiSWIFTfi Drifters, *Journal of Atmospheric and Oceanic Technology*, 29(12), 1866–1882, doi:10.1175/JTECH-D-12-00018.1, 2012.
- Thomson, J., Wave propagation in the marginal ice zone: Connections and feedback mechanisms within the air ice ocean system, *Phil. Trans. R. Soc. A*, 380(20210251), doi:10.1098/rsta.2021.0251, 2022.
- Thomson, J., and W. E. Rogers, Swell and sea in the emerging Arctic Ocean, *Geophys. Res. Lett.*, 41, 3136–3140, doi:10.1002/2014GL059983, 2014.
- Thomson, J., J. B. Girton, R. Jha, and A. Trapani, Measurements of directional wave spectra and wind stress from a Wave Glider autonomous surface vehicle, *J. Atmos. Ocean. Technol.*, 35(2), 347–363, doi:10.1175/JTECH-D-17-0091.1, 2018a.
- Thomson, J., et al., Emerging trends in the sea state of the Beaufort and Chukchi seas, *Ocean Model.*, 105, doi:10.1016/j.ocemod.2016.02.009, 2016.
- Thomson, J., et al., Overview of the Arctic Sea State and Boundary Layer Physics Program, *J. Geophys. Res.*, 123(12), 8674–8687, doi:10.1002/2018JC013766, 2018b.
- Tolman, H. L., A third generation model for wind-waves on slowly varying, unsteady, and inhomogeneous depths and currents, *J. Phys. Oceanogr.*, 21(6), 782–797, 1991.
- Wang, Y., B. Holt, W. E. Rogers, J. Thomson, and H. H. Shen, Wind and wave influences on sea ice floe size and leads in the Beaufort and Chukchi seas during the summer-fall transition 2014, *J. Geophys. Res.*, 121, 1502–1525, doi:10.1002/2015JC011349, 2016.



RADARSAT-2 Imagery Copyright © 2014 MacDonald, Dettwiler and Associates LTD. All rights reserved.



RADARSAT-2 Imagery Copyright © 2014 MacDonald, Dettwiler and Associates LTD. All rights reserved.

Figure 1: Satellite ice products annotated by the U.S. National Ice Center as a special support product for the Marginal Ice Zone project. APL-UW TR 2302

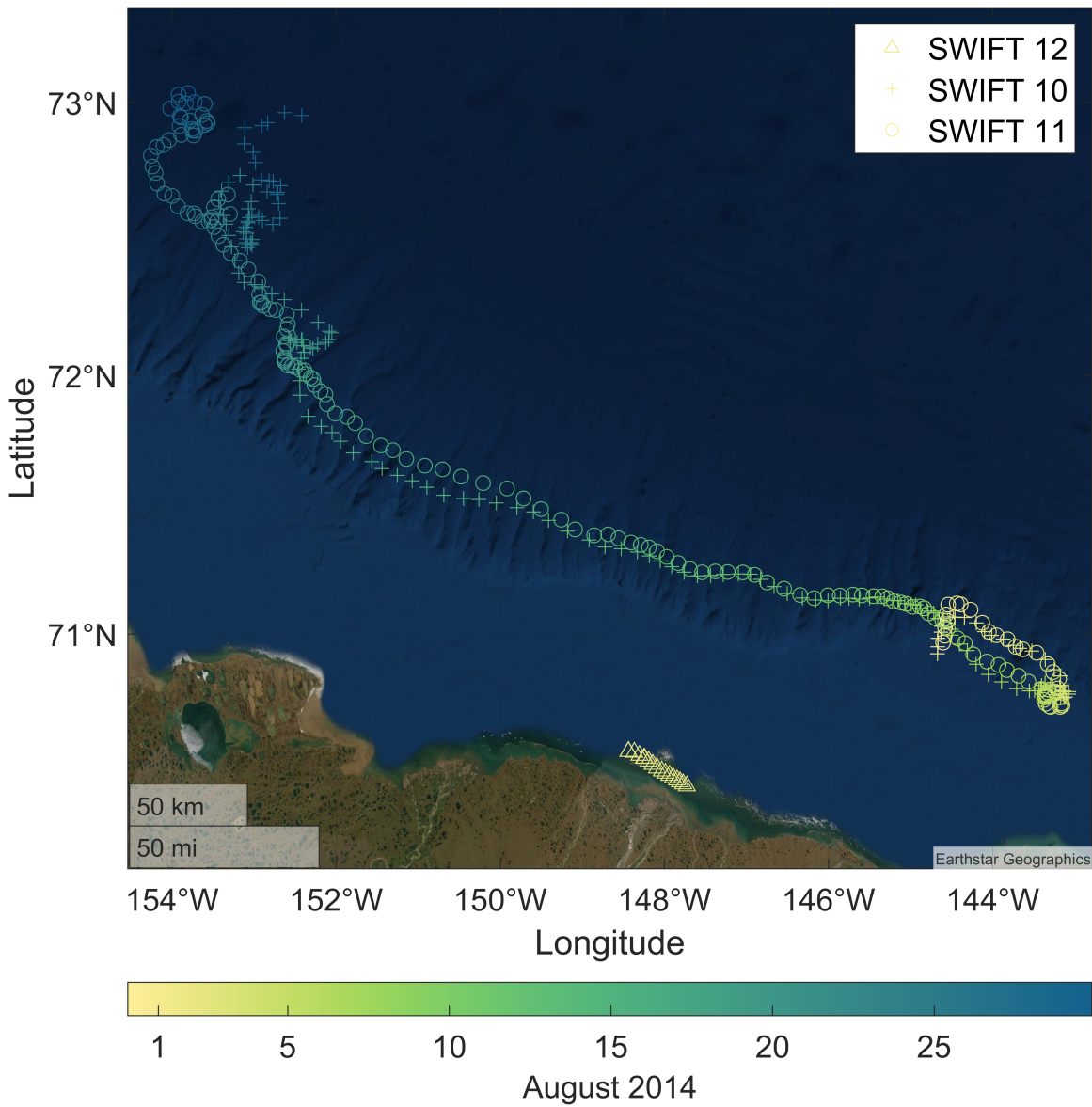


Figure 2: Trajectories of three SWIFT buoys deployed in August 2014 off the northern coast of Alaska.



Figure 3: SWIFT 12 in Stefansson Sound on 2 August 2014, initially deployed near a large ice floe (left) and later re-positioned approximately 6 km farther along a fetch of partially open water (right).

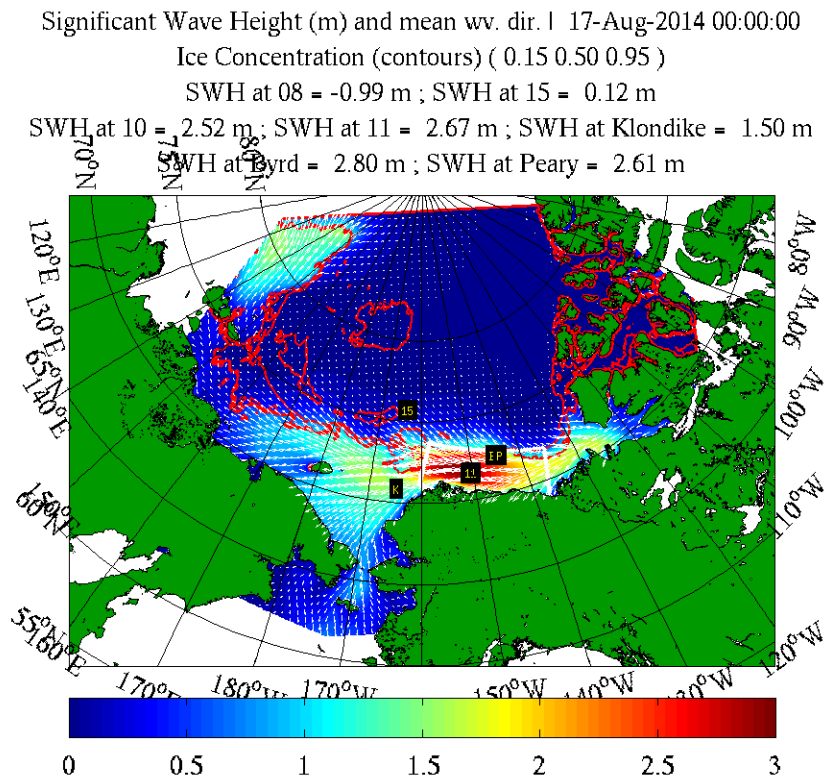


Figure 4: Results from a WAVEWATCH III simulation used to provide boundary forcing for SWAN, for 17 August 2014 0000 UTC. Colors indicate significant waveheight. Arrows indicate mean wave direction. Contours are for ice concentrations of 15%, 50%, and 95%. Black markers indicate buoy positions. Observed waveheights are indicated in text above plot. White dotted line indicates SWAN nest.

Significant Wave Height (m) and mean wv. dir. | 17-Aug-2014 00:00:00  
Ice Concentration (contours) ( 0.15 0.50 0.95 )  
SWH at 08 = -0.99 m ; SWH at 15 = 0.12 m  
SWH at 10 = 2.52 m ; SWH at 11 = 2.67 m ; SWH at Klondike = 1.50 m  
SWH at Byrd = 2.80 m ; SWH at Peary = 2.61 m

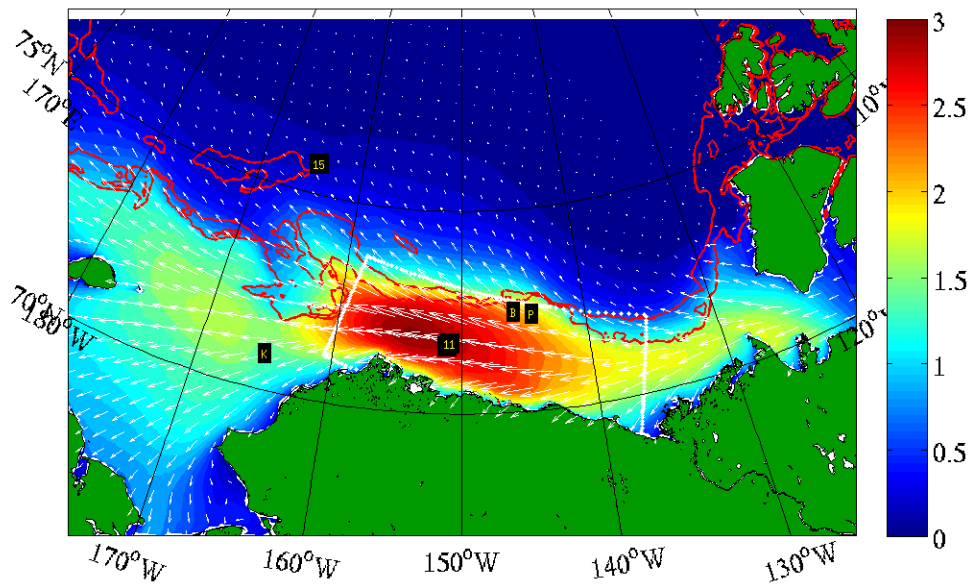


Figure 5: As in Figure 4, but zoomed in for better view of the SWAN nest region.

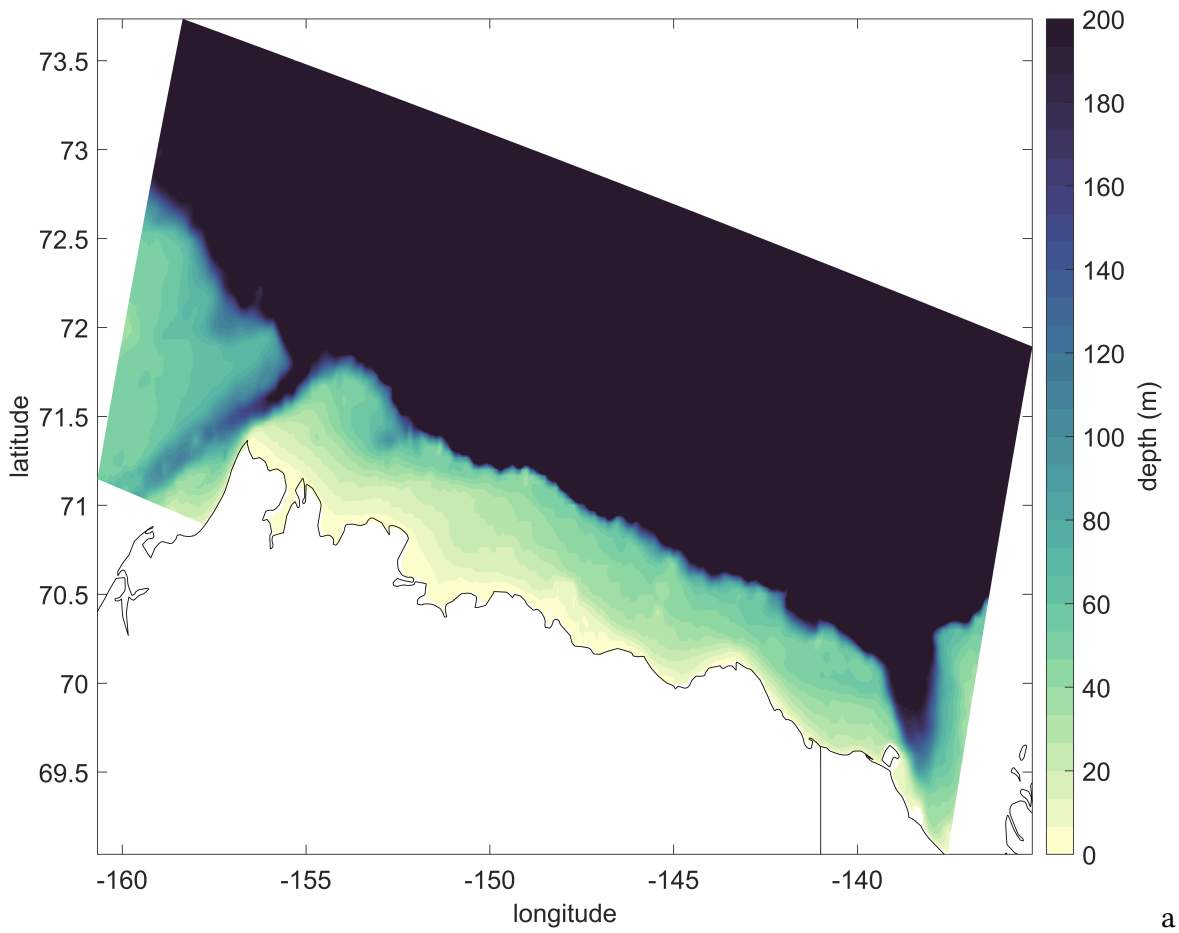


Figure 6: Computational domain used for the SWAN model runs. Color bar shows the ocean bathymetry sourced from ETOPO1 Global Relief Model [Amante, C., and B.W. Eakins (2009)].

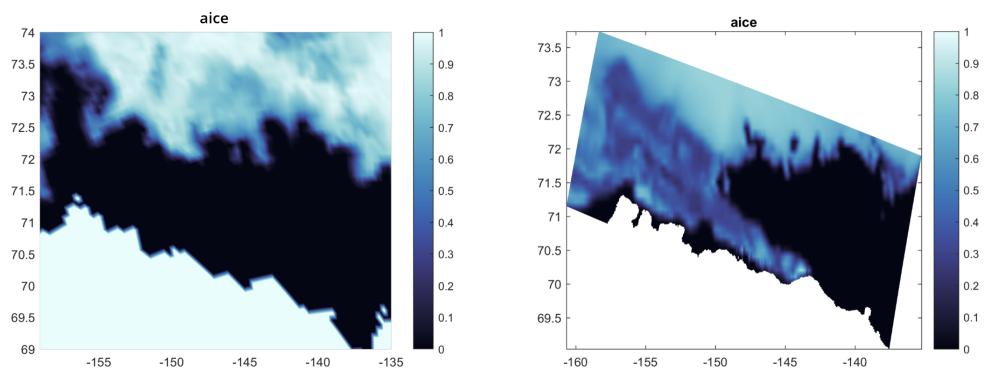


Figure 7: Sea ice concentration reported in the study area by the AMSR2 (left) and Arctic Cap (right) products on 2 August 2014. AMSR2 does not resolve the remnant coastal ice that is essential to this case study.

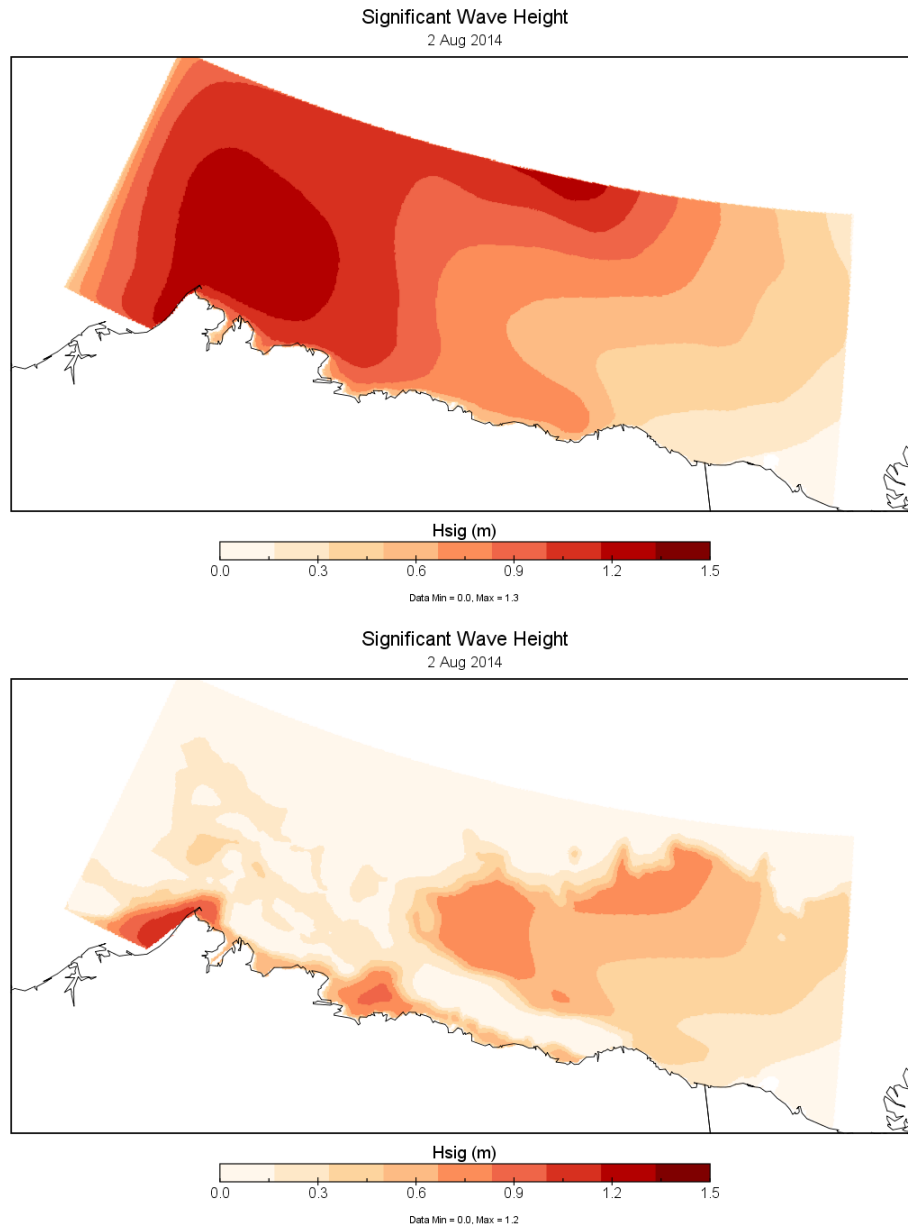


Figure 8: Maps of significant wave height on 2 August 2014 from two SWAN model runs: without ice source term (top) and with IC4M2 ice source term forced by the Arctic Cap ice product (bottom).

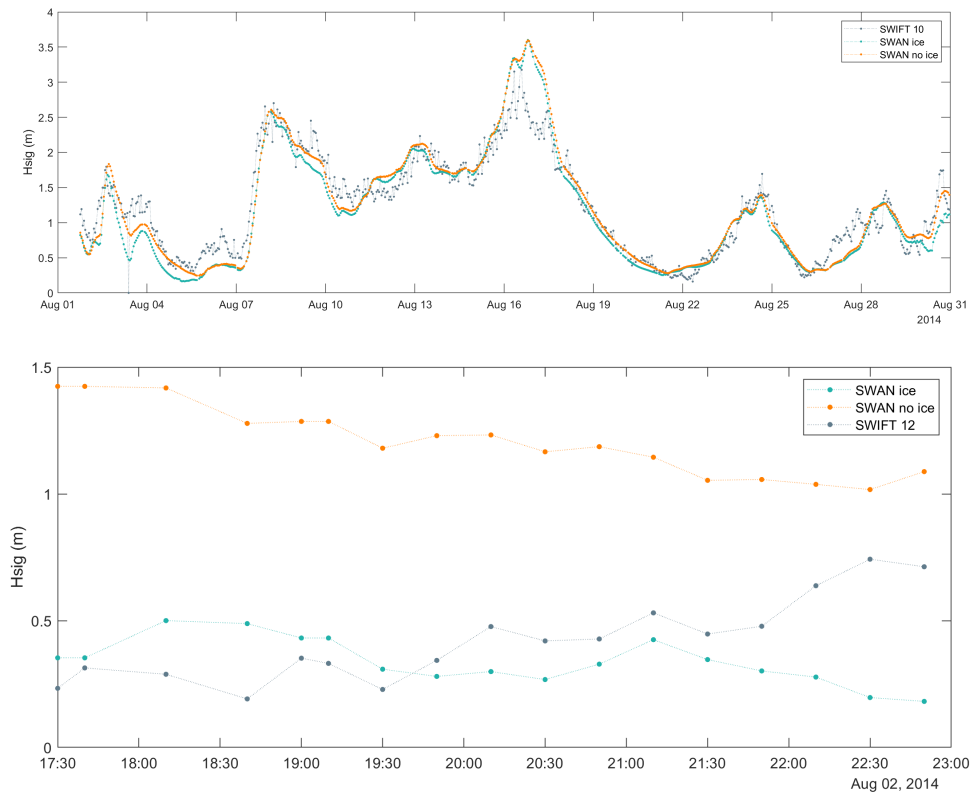


Figure 9: Top: Significant wave height measured by SWIFT 10 deployed throughout August 2014, compared to SWAN model runs with and without the sea ice source term  $S_{ice}$ . Model results are evaluated at the nearest grid cell/time step to the buoy coordinates. Bottom: Same as above, but for SWIFT 12 in Stefansson Sound on 2 August 2014.

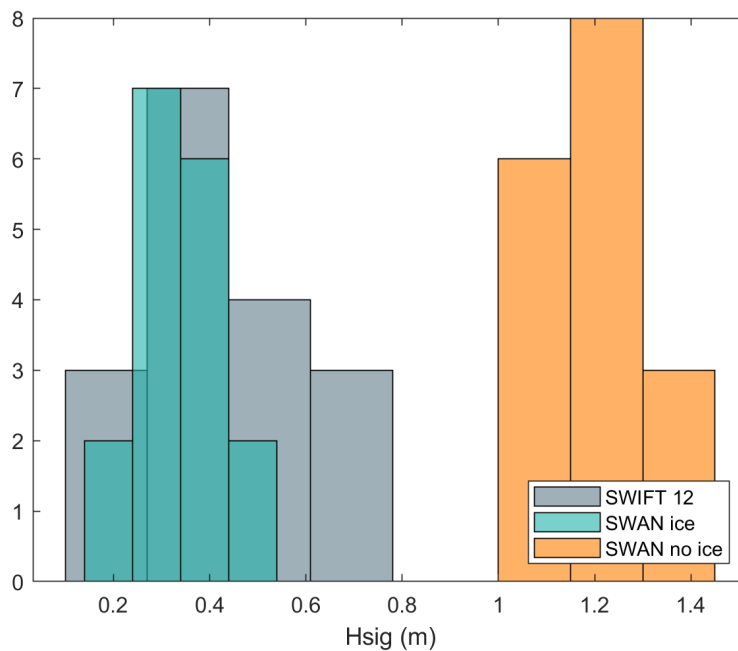


Figure 10: Histogram of instances of significant wave heights observed by SWIFT 12 on 2 August 2014 compared to SWAN model results with and without the sea ice attenuation scheme.

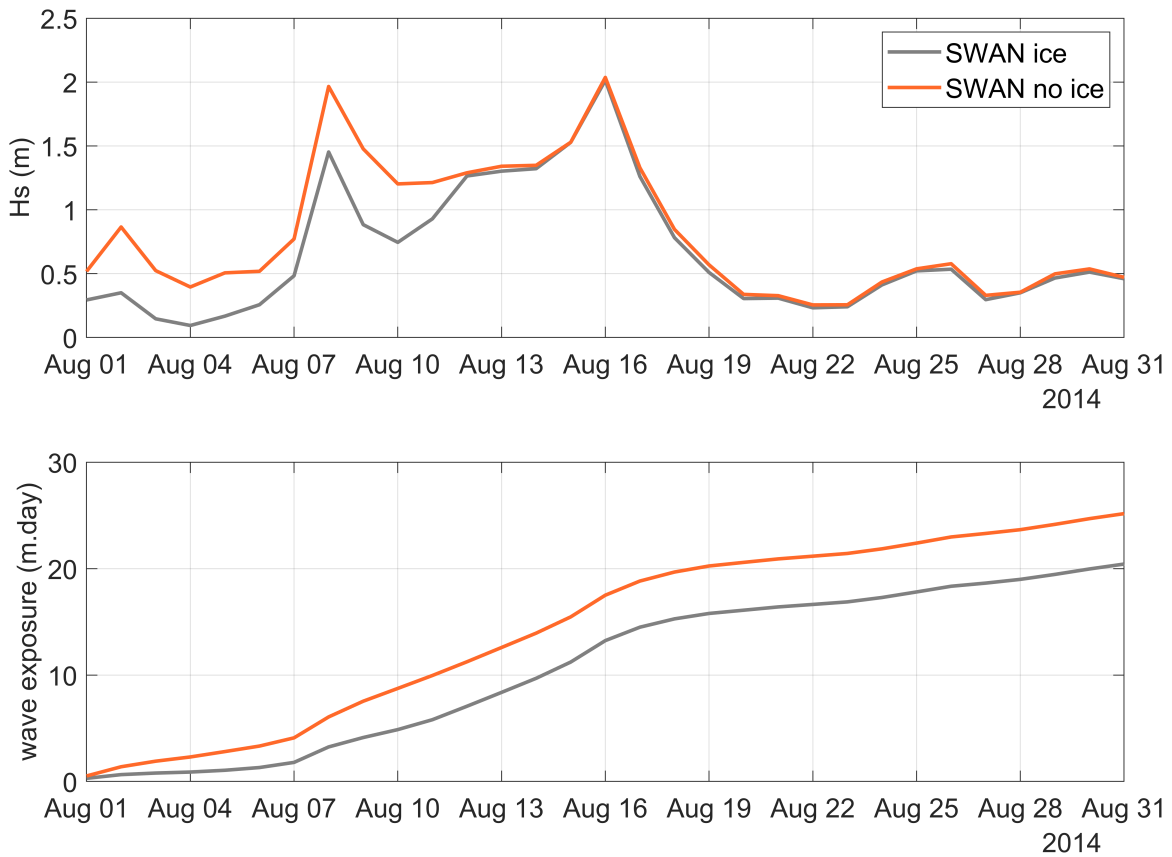


Figure 11: Top: Mean significant wave height of the southern-most grid cells with > 10 m water depth within the SWAN domain, estimated using the two runs outlined in section 4.1. Bottom: Same as above, but accumulated daily over the month of August 2014.